0026-895X/10/7801-81–93$20.00
MOLECULAR PHARMACOLOGY
Copyright © 2010 The American Society for Pharmacology and Experimental Therapeutics
Mol Pharmacol 78:81–93, 2010

Vol. 78, No. 1
64584/3600491
Printed in U.S.A.

Mapping the Binding Pocket of Dual Antagonist Almorexant to Human Orexin 1 and Orexin 2 Receptors: Comparison with the Selective OX_1 Antagonist SB-674042 and the Selective OX_2 Antagonist *N*-Ethyl-2-[(6-methoxy-pyridin-3-yl)-(toluene-2-sulfonyl)-amino]-*N*-pyridin-3-ylmethyl-acetamide (EMPA)

Pari Malherbe, Olivier Roche, Anne Marcuz, Claudia Kratzeisen, Joseph G. Wettstein, and Caterina Bissantz

Psychiatry Disease Area (P.M., A.M., C.K., J.G.W.) and Chemistry Discovery (O.R., C.B.), F. Hoffmann-La Roche Ltd., Basel, Switzerland

Received March 9, 2010; accepted April 16, 2010

ABSTRACT

The orexins and their receptors are involved in the regulation of arousal and sleep–wake cycle. Clinical investigation with almorexant has indicated that this dual OX antagonist is efficacious in inducing and maintaining sleep. Using site-directed mutagenesis, β_2-adrenergic-based OX_1 and OX_2 modeling, we have determined important molecular determinants of the ligand-binding pocket of OX_1 and OX_2. The conserved residues $Asp^{45.51}$, $Trp^{45.54}$, $Tyr^{5.38}$, $Phe^{5.42}$, $Tyr^{5.47}$, $Tyr^{6.48}$, and $His^{7.39}$ were found to be contributing to both orexin-A-binding sites at OX_1 and OX_2. Among these critical residues, five (positions 45.51, 45.54, 5.38, 5.42, and 7.39) were located on the C-terminal strand of the second extracellular loop (ECL2b) and in the top of TM domains at the interface to the main binding crevice, thereby suggesting superficial OX receptor interactions of orexin-A. We found that the mutations $W214A^{45.54}$, $Y223A^{5.38}$, $F227A^{5.42}$, $Y317A^{6.48}$, and $H350A^{7.39}$ resulted in the complete loss of both [^{3}H]almorexant and [^{3}H]*N*-ethyl-2-[(6-methoxy-pyridin-3-yl)-(toluene-2-sulfonyl)-amino]-*N*-pyridin-3-ylmethyl-acetamide (EMPA) binding affinities and also blocked their inhibition of orexin-A-evoked $[Ca^{2+}]_i$ response at OX_2. The crucial residues $Gln126^{3.32}$, $Ala127^{3.33}$, $Trp206^{45.54}$, $Tyr215^{5.38}$, $Phe219^{5.42}$, and $His344^{7.39}$ are shared between almorexant and 1-(5-(2-fluoro-phenyl)-2-methyl-thiazol-4-yl)-1-((*S*)-2-(5-phenyl-(1,3,4)oxadiazol-2-ylmethyl)-pyrrolidin-1-yl)-methanone (SB-674042) binding sites in OX_1. The nonconserved residue at position 3.33 of orexin receptors was identified as occupying a critical position that must be involved in subtype selectivity and also in differentiating two different antagonists for the same receptor. In summary, despite high similarities in the ligand-binding pockets of OX_1 and OX_2 and numerous aromatic/hydrophobic interactions, the local conformation of helix positions 3.32, 3.33, and 3.36 in transmembrane domain 3 and 45.51 in ECL2b provide the structural basis for pharmacologic selectivity between OX_1 and OX_2.

The hypothalamic neuropeptides orexin-A/hypocretin-1 (33 amino acids) and orexin-B/hypocretin-2 (28 amino acids) are derived from the proteolytic processing of 130 amino acids prepro-orexin (Sakurai et al., 1998; de Lecea et al., 1998). Orexin peptides elicit their effect through two G-protein-coupled receptors (GPCRs) called OX_1 and OX_2 (nomenclature follows Alexander et al., 2008) that couple to $G_{q/11}$ and contribute to the activation of phospholipase C, leading to the elevation of intracellular Ca^{2+} concentrations (Sakurai et al., 1998). However, a detailed signaling profile of the hOX_2 has recently shown that OX_2 could couple to G_s as well as $G_{q/11}$ and G_i pathways (Tang et al., 2008). The binding and func-

Article, publication date, and citation information can be found at http://molpharm.aspetjournals.org.
doi:10.1124/mol.110.064584.

ABBREVIATIONS: GPCR, G-protein coupled receptor; OX_1, orexin 1 receptor; OX_2, orexin 2 receptor; almorexant, (2*R*)-2-{(1*S*)-6,7-dimethoxy-1-[2-(4-trifluoromethyl-phenyl)-ethyl]-3,4-dihydro-1*H*-isoquinolin-2-yl}-*N*-methyl-2-phenyl-acetamide (ACT-078573); EMPA, *N*-ethyl-2-[(6-methoxy-pyridin-3-yl)-(toluene-2-sulfonyl)-amino]-*N*-pyridin-3-ylmethyl-acetamide; SB-674042, 1-(5-(2-fluoro-phenyl)-2-methyl-thiazol-4-yl)-1-((*S*)-2-(5-phenyl-(1,3,4)oxadiazol-2-ylmethyl)-pyrrolidin-1-yl)-methanone; 3D, three-dimensional; TM, transmembrane; 7TMD, seven-transmembrane domain; $[Ca^{2+}]_i$, cytosolic free Ca^{2+} concentration; FLIPR, fluorometric imaging plate reader; AR, adrenergic receptor; WT, wild type; NK, neurokinin receptor; PDB, Protein Data Bank; BSA, bovine serum albumin; HEK, human embryonic kidney; ECL, extracellular loop; NSB, nonspecific binding; SB, specific binding.

tional characterization demonstrated that orexin-B has a 10-fold lower affinity for the OX_1 over the OX_2, whereas orexin-A and orexin-B bind to OX_2 with similar affinities (Sakurai et al., 1998).

Distribution studies in rat brain using in situ hybridization and immunohistochemistry have shown that orexin neurons are found exclusively in the lateral hypothalamic area, having projections to the entire central nervous system (Peyron et al., 1998; Nambu et al., 1999). OX_1 and OX_2 receptors are differentially expressed in the CNS. Although both receptors are present in most brain regions such as neocortex L6, ventral tegmental area, preoptic area, dorsal and medial raphe nuclei, periaqueductal area and hypothalamus, OX_1 is most abundantly expressed in the locus ceruleus, whereas OX_2 is expressed in regions controlling arousal, especially in the tuberomammillary nucleus, an important site for the regulation of sleep/wakefulness (Trivedi et al., 1998; Marcus et al., 2001).

The orexin system has been implicated in numerous physiological functions, including energy homeostasis, feeding and reward, regulation of arousal, and the sleep-wake cycle (Kilduff and Peyron, 2000; Ohno and Sakurai, 2008). Preclinical (canine and rat) and clinical (healthy male subjects; single dose) investigations have shown that almorexant, when administered orally during the active period, promoted sleep in animals and humans without disrupting the sleep architecture or inducing cataplexy (Brisbare-Roch et al., 2007; Neubauer, 2010), thereby further validating the involvement of orexin system in the regulation of alertness and sleep. Thus, OX antagonists represent an alternative therapeutic approach for the treatment of insomnia (Nishino, 2007; Roecker and Coleman, 2008; Boss et al., 2009). The biochemical characterization of EMPA, a high-affinity, reversible, and in vivo active OX_2 antagonist with 900-fold selectivity in binding for OX_2 over OX_1, has been reported (Malherbe et al., 2009a). Furthermore, the biochemical characterization of almorexant (a high-affinity dual OX_1/OX_2) has demonstrated that it had an apparent noncompetitive and long-lasting pseudo-irreversible mode of antagonism that was due to its very slow rate of dissociation from OX_2, whereas it displayed a competitive mode of antagonism at OX_1 (Malherbe et al., 2009b). 1-(5-(2-Fluoro-phenyl)-2-methyl-thiazol-4-yl)-1-((*S*)-2-(5-phenyl-(1,3,4)oxadiazol-2-ylmethyl)-pyrrolidin-1-yl)-methanone (SB-674042), which is a high-affinity and selective OX_1 antagonist (Langmead et al., 2004), has been also shown to behave in an apparent noncompetitive manner at hOX_1 similar to that of almorexant at hOX_2 (Malherbe et al., 2009b).

Several researchers, who have investigated the determinants of orexin-A required to activate OX_1 and OX_2 using truncated peptides and alanine-scanned peptides (systematic replacement of the natural amino acids with L-alanine) (Ammoun et al., 2003; Lang et al., 2004, 2006; Takai et al., 2006) have indicated that: 1) a minimal 19 amino acids of C-terminal segment of orexin-A (Arg15-Leu33) is required for OX activation, though functional activity of this peptide is reduced; 2) the replacement of orexin-A (Arg15–Leu33) truncated peptide residues, Leu16, Leu19, Leu20, His26, Gly29, Ile30, Leu31, Thr32, and Leu33 with alanine led to a significant reduction in the functional potency at the OX_1 (Darker et al., 2001); and 3) orexin-A distinctly recognized OX_1 from OX_2 and its binding to OX_1 required more molecular determinants than binding to OX_2. Thus far, little is known about the OX ligand-binding pocket. The current research used a combination of β2AR-based OX_1 and OX_2 modeling; site-directed mutagenesis; [^{3}H]almorexant, [^{3}H]EMPA, and [^{3}H]SB-674042 bindings; and orexin-A evoked intracellular calcium mobilization fluorometric imaging plate reader (FLIPR) assay to probe the antagonist-binding site of OX_1 and OX_2. Amino acid residues in the TM3, -5, -6, -7, and ECL2b regions, initially identified from an alignment of the seven-transmembrane domain (7TMD) of OX_1 and OX_2 with hβ2AR, were demonstrated by mutational analysis to be important determinants of the high-affinity antagonist-binding pocket of the OX_1 and OX_2. Furthermore, these experimental findings allow the construction of homology models of OX_1- and OX_2-7TMD based on the X-ray crystal of hβAR (PDB id code 2RH1; Cherezov et al., 2007; Rosenbaum et al., 2007) and suggest possible binding modes for EMPA-OX_2, SB-674042–OX_1, and almorexant-OX_1 and -OX_2 complexes.

Materials and Methods

Materials. Almorexant (ACT-078573) (Brisbare-Roch et al., 2007), EMPA (Malherbe et al., 2009a), and SB-674042 (Langmead et al., 2004) were synthesized in the Chemistry Department of F. Hoffmann-La Roche. [^{3}H]Almorexant (specific activity, 42.7 Ci/mmol), [^{3}H]EMPA (specific activity, 94.3 Ci/mmol), and [^{3}H]SB-674042 (specific activity, 24.4 Ci/mmol) (Fig. 1A) were synthesized by Drs. Philipp Huguenin and Thomas Hartung at the Roche chemical and isotope laboratories (Basel, Switzerland). Orexin-A (Fig. 1B) was purchased from Tocris Bioscience (Bristol, UK).

Construction of Point-Mutated hOX_1 and hOX_2 Receptors. cDNA encoding human OX_1 (Swiss-Prot accession no. O43613) and human OX_2 (Swiss-Prot accession no. O43614) were subcloned into pCI-Neo expression vectors (Promega, Madison, WI). All point mutants were constructed by using the QuikChange site-directed mutagenesis kit (Stratagene, La Jolla, CA) according to the manufacturer's instructions and by using pCI-Neo-hOX_1 or pCI-Neo-hOX_2 as a DNA template. Complementary oligonucleotide primers (sense and antisense) containing the single site of mutation were synthesized by Microsynth AG (Balgach, Switzerland). The following polymerase chain reaction conditions were used for repeated extensions of the plasmid template: 95°C for 1 min and 20 cycles of 95°C for 30 s, 55°C for 1 min, and 68°C for 8 min using 50 ng of plasmid DNA, 100 ng of each primer, and 2.5 units of *Pfu* Turbo DNA polymerase (Stratagene). The entire coding regions of all positive point mutants were sequenced from both strands using an automated cycle sequencer (Applied Biosystems, Foster City, CA).

Cell Culture and Membrane Preparation. HEK293 cells were transfected as described previously (Malherbe et al., 2009a). Forty-eight hours after transfection, cells were harvested and washed three times with cold phosphate-buffered saline and frozen at −80°C. The pellet was suspended in ice-cold buffer containing 15 mM Tris-HCl, pH 7.5, 2 mM $MgCl_2$, 0.3 mM EDTA, 1 mM EGTA, and protease inhibitor cocktail EDTA-free (Roche Applied Science, Rotkreuz, Switzerland) and homogenized with a Polytron homogenizer (Kinematica AG, Basel, Switzerland) for 30 s at 16,000 rpm. After centrifugation at 48,000*g* for 30 min at 4°C, the pellet was suspended in ice-cold buffer containing 75 mM Tris-HCl, pH 7.5, 12.5 mM $MgCl_2$, 0.3 mM EDTA, 1 mM EGTA, 250 mM sucrose, and protease inhibitor cocktail EDTA-free. The membrane homogenate was frozen at −80°C before use.

[^{3}H]Almorexant, [^{3}H]EMPA, and [^{3}H]SB-674042 Bindings. After thawing, membrane homogenates were centrifuged at 48,000*g* for 10 min at 4°C, the pellets were resuspended in the binding buffer (1× Hanks' balanced salt solution, 20 mM HEPES, pH 7.4, and 0.1%

BSA) to a final assay concentration of 5 μg of protein/well. Saturation isotherms were determined by addition of various concentrations of [^{3}H]almorexant (0.02–20 nM at OX_1, 0.03–15 nM at OX_2R), [^{3}H]EMPA (0.01–12 nM at OX_2), or [^{3}H]SB-674042 (0.03–15 nM at OX_1) to these membranes (in a total reaction volume of 500 μl). The incubation time for [^{3}H]almorexant and [^{3}H]SB-674042 on OX_1 membranes was 90 min at 23°C. The incubation for [^{3}H]almorexant and [^{3}H]EMPA on OX_2-expressing membrane was 120 min and 60 min at 23°C, respectively. At the end of incubation, membranes were filtered onto unitfilter (96-well white microplate with bonded GF/C filter preincubated for 1 h in wash buffer plus 0.5% polyethylenimine and 0.1% BSA) with a Filtermate 196 harvester (PerkinElmer Life and Analytical Sciences, Waltham, MA) and washed four times with ice-cold wash buffer (1 × Hanks' balanced salt solution and 20 mM HEPES, pH 7.4). Nonspecific bindings for [^{3}H]almorexant, [^{3}H]EMPA, and [^{3}H]SB-674042 were measured in the presence of 10 μM almorexant, EMPA, and SB-674042, respectively. Radioactivity on the filter was counted (5 min) on a TopCount microplate scintillation counter (PerkinElmer Life and Analytical Sciences) with quenching correction after addition of 45 μl of MicroScint 40 (PerkinElmer Life and Analytical Sciences) and shaking for 1 h. Saturation experiments were analyzed by Prism 5.0 (GraphPad Software, San Diego, CA) using the rectangular hyperbolic equation derived from the equation of a bimolecular reaction and the law of mass action, $B = (B_{max} \cdot [F])/(K_d + [F])$, where B is the amount of ligand bound at equilibrium, B_{max} is the maximum number of binding sites, [F] is the concentration of free ligand, and K_d is the ligand dissociation constant. For all mutants, the experiments were performed three to five times in triplicate, and the mean ± S.E. of the individual K_d and B_{max} values were calculated and are reported. Statistical significance was determined using the two-tailed t test (Prism 5.0).

Intracellular Ca^{2+} Mobilization Assay. HEK293 cells, which were grown to 80% confluence in growth medium (Dulbecco's modified Eagle's medium high glucose supplemented with 10% fetal calf serum and 100 μg/μl penicillin/streptomycin), were transfected with the wild-type or mutant orexin receptor cDNAs in pCI-Neo using Lipofectamine Plus reagent (Invitrogen, Carlsbad, CA) according to the manufacturer's instruction. Six hours after transfection, the DNA-transfection mixture was removed, and the cells were maintained in growth medium. Twenty-four hours after transfection, the cells were harvested and seeded at 6×10^4 cells/well in the poly-D-lysine–treated, 96-well, black/clear-bottomed plates (BD Biosciences, Palo Alto, CA). Forty-eight hours after transfection, the cells were loaded for 1 h at 37°C with 4 μM Fluo-4 acetoxymethyl ester (Invitrogen, Carlsbad, CA) in loading buffer (1× Hanks' balanced salt solution and 20 mM HEPES). The cells were washed five times with loading buffer to remove excess dye, and $[Ca^{2+}]_i$ was measured using a FLIPR (Molecular Devices, Sunnyvale, CA) as described previously (Malherbe et al., 2009b). Orexin-A (50 mM stock solution in dimethyl sulfoxide) was diluted in FLIPR buffer plus 0.1% BSA. The EC_{50} and EC_{80} values of orexin-A were measured daily from standard agonist concentration-response curves in HEK293 cells transiently transfected with the WT or mutant orexin receptors. Inhibition curves were determined by addition of 11 concentrations (0.0001–10 μM in FLIPR buffer) of inhibitory compounds and using EC_{80} value of orexin-A as agonist (a concentration that gave 80% of maximum agonist response, determined daily). The antagonists were applied 25 min (incubation at 37°C) before the application of the agonist. Responses were measured as peak increase in fluorescence minus basal, normalized to the maximal stimulatory effect induced by EC_{80} value of orexin-A. Inhibition curves were fitted according to the Hill equation: $y = 100/(1 + (x/IC_{50})^{nH})$, where n_H = slope factor using Prism 5.0. K_b values were calculated according to the following equation: $K_b = IC_{50}/(1 + [A]/EC_{50})$, where A is the concentration of agonist added that is very close to agonist EC_{80} value, and IC_{50} and EC_{50} values were derived from the antagonist inhibition and orexin agonist curves, respectively. The relative efficacy (E_{max}) values of orexin-A was calculated as fitted maximum of the dose-response curve of each mutated receptors expressed as a percentage of fitted maximum of the wild type dose-response curve from cells transfected and assayed on the same day.

Residue Numbering Scheme. The position of each amino acid residue in the 7TMD was identified both by its sequence number and by its generic number proposed by Ballesteros and Weinstein (1995). In this numbering system, amino acid residues in the 7TMD are given two numbers; the first refers to the transmembrane (TM) number (1–7), the second one indicates the relative position relative to a highly conserved residue in class A GPCRs in that TM, which is arbitrarily assigned 50. The second extracellular loop (ECL2) is labeled 45 to indicate its location between helices 4 and 5, and the conserved cysteine thought to be disulfide-bonded is given index number 45.50. The residues within the ECL2 loop are then indexed relative to this position. ECL2b is the C-terminal strand of ECL2 that connects $Cys^{3.25}$ with $Cys^{45.50}$.

Alignment and Model Building. The amino acid sequences of the human OX_1 (O43613) and human OX_2 (O43614) were retrieved from the Swiss-Prot database. A model was built by aligning the 7TMs and ECL2 of orexin receptor sequences on the β2-adrenergic receptor (Swiss-Prot accession no. P07550) sequence to use the 2.4-Å high-resolution crystal structure determined by Cherezov et al. (2007) as a template (PDB code 2RH1). The initial alignment was generated with the ClustalW multiple alignment program using the BLOSUM matrix and then manual inspection was performed to ensure that conserved residues were aligned. Then, the software package MOE (version 2005.05; Chemical Computing Group, Montreal, Quebec, QC, Canada) was used to create 3D models of human OX_1 and OX_2 based on β2AR (PDB code 2RH1). Ten intermediates were generated and the best model was selected. No minimization was performed to keep the backbone coordinates of the crystallographic structure. The three molecules (SB-674042, EMPA, and almorexant) were then manually docked into the membrane cavity. The binding site was defined as the set of amino acids found at 6.0Å away from the carazolol in the X-ray structure of β2-adrenergic receptor.

Results

Binding Characteristics of [^{3}H]SB-674042, [^{3}H]EMPA, and [^{3}H]Almorexant. To investigate the 7TMD pocket of OX_1 and OX_2 receptors, three radioligand antagonists, [^{3}H]SB-674042, [^{3}H]EMPA, and [^{3}H]almorexant, were selected for the current study (Fig. 1A). [^{3}H]SB-674042 is the first radioligand antagonist selective for hOX_1 to be described (Langmead et al., 2004). In the filtration binding assay, [^{3}H]SB-674042 has displayed high-affinity binding to hOX_1 with a K_d value of 0.74 nM. SB-674042 has also showed a 275-fold selectivity in functional assay (FLIPR) for hOX_1 over

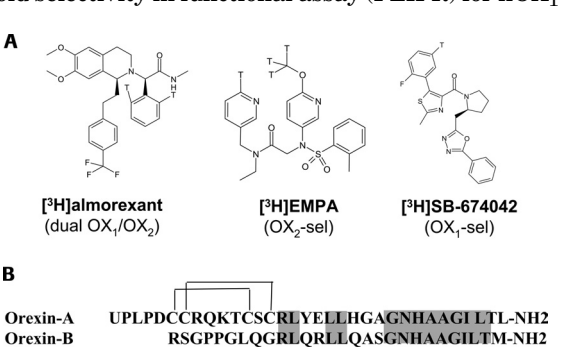

Fig. 1. A, chemical structures of the selective OX_1, OX_2, and dual OX_1/OX_2 antagonists. T, tritium. B, the amino acid sequences of orexin-A and -B. Orexin-A has a pyroglutamate (2-pyrrolidone-5-carboxylic acid) at the first N-terminal residue site, which is indicated by U. The C termini of both orexins (-NH_2) are amidated. Two intramolecular disulfide bonds in orexin-A formed between C6 and C12 and are shown between C7 and C14 as lines. The residues identical in both orexins are highlighted in gray.

hOX_2 (Malherbe et al., 2009b). The biochemical characterization of an OX_2 antagonist, EMPA, with 900-fold selectivity in binding for OX_2 over OX_1 has been reported (Malherbe et al., 2009a). [^{3}H]EMPA is a high-affinity radioligand that binds to HEK293-hOX_2 membrane with K_d value of 1.1 nM. [^{3}H]Almorexant bound with high affinity to a single saturable site on recombinant hOX_1 and hOX_2 with K_d values of 1.3 and 0.17 nM at 37°C, respectively (Malherbe et al., 2009b). Furthermore, SB-674042 and EMPA were able to displace the [^{3}H]almorexant binding from hOX_1 and hOX_2 membranes with K_i values of 1.9 and 1.2 nM, respectively. Therefore, it is concluded that almorexant should share a common binding pocket in the transmembrane region of the orexin receptors or at least overlapping with those of SB-674042 on hOX_1 and EMPA on hOX_2.

Alignment of 7TM Domains of the OX Receptors toward hβ2AR and Selection of the Orexin Receptor Mutations. The orexin receptors are highly conserved across mammalian species. Human OX_1 and OX_2 display 64% overall sequence identity (Sakurai et al., 1998); an even higher degree of identity of 84% is found when comparing 7TMD regions (Fig. 2). To elucidate the binding modes of almorexant, EMPA, and SB-674042, an alignment of the seven transmembrane helices of the hOX_1 and hOX_2 toward the transmembrane helices of human β2-adrenergic receptor (PDB id code 2RH1) (Cherezov et al., 2007; Rosenbaum et al., 2007)

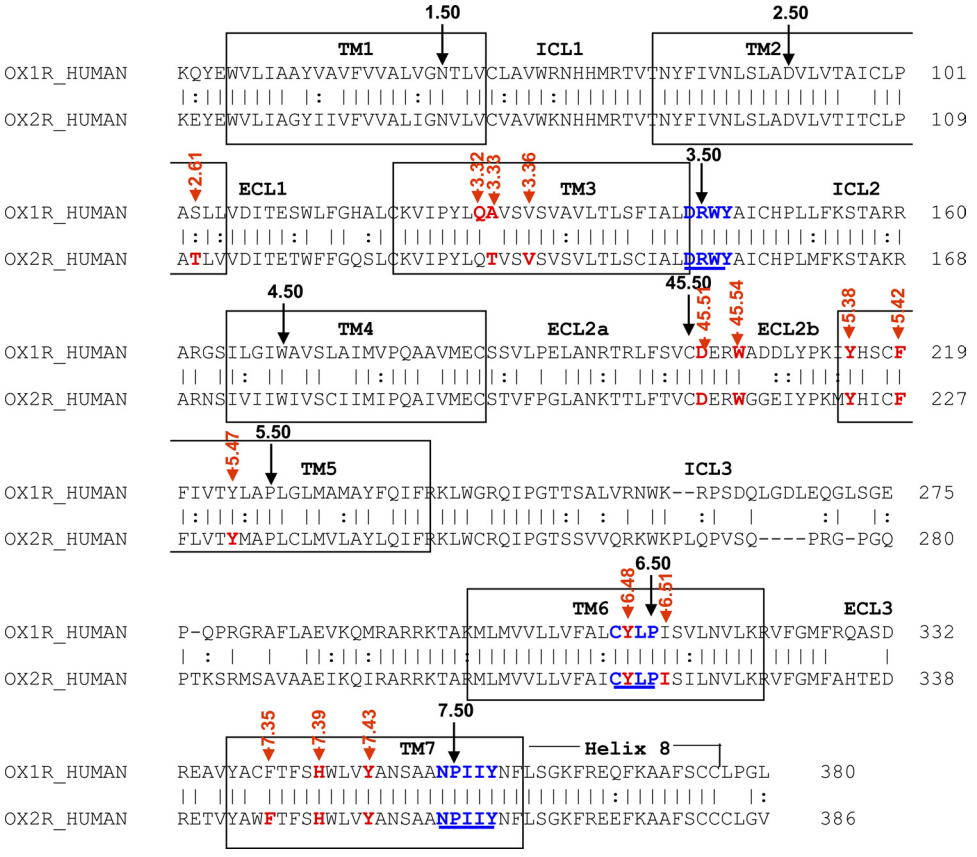

Fig. 2. Amino acid sequence alignment of the TM1–Helix 8 region of the hOX_1 with the hOX_2 using pairwise global alignment (Needleman-Wunsch algorithm). The numbers on the right refer to the amino acids of hOX_1 and hOX_2 receptors. Vertical lines indicate identical residues and colons indicate conservative replacement of residues (chemically homologous residues) between hOX_1 and OX_2. The TM domains are boxed. The conserved residue in each TM that is assigned to 50 according to the Ballesteros-Weinstein numbering scheme is shown by black arrows. The critical residues (as indicated by the Ballesteros-Weinstein numbering scheme) in the binding pocket of orexin receptor antagonists (almorexant, EMPA, SB-674042) are shown by red boldface type and red short arrows. Three conserved motifs in TM3 (DRY), TM6 (CWxP), and TM7 (NPxxY), which are believed to function as microswitches (Nygaard et al., 2009), are shown in blue boldface type and underlined. ICL, intracellular loop.

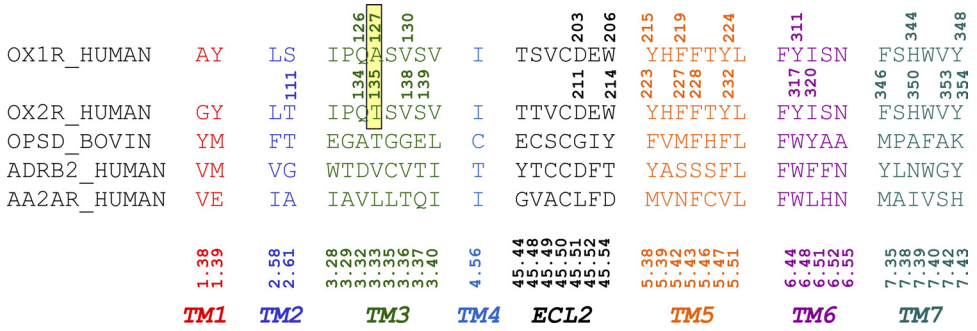

Fig. 3. Alignment of the amino acids forming the binding site of OX_1 and OX_2 relative to bovine rhodopsin (Swiss-Prot accession no. P02699), human β_2-adrenergic (Swiss-Prot accession no. P07750), and human A_{2A} adenosine (Swiss-Prot accession no. P29274) receptors. Ballesteros-Weinstein numbering scheme of the amino acids (indicated above the TMs in the bottom row) are given to facilitate the comparison with other GPCRs (see *Materials and Methods*). The numbers above the OX1R_HUMAN and OX2R_HUMAN receptors give the sequence number of the positions of the mutations carried out in this study. The residues at helix position 3.33, which are different in OX_1 and OX_2 binding pockets, are boxed and highlighted yellow.

was made (Fig. 3). In Fig. 3, an alignment of 7TM of the hOX_1 and hOX_2 toward the 7TM of bovine rhodopsin (PDB id code 1F88) (Palczewski et al., 2000) and human A_{2A} adenosine receptor (PDB id code 3EML) (Jaakola et al., 2008) were also shown for comparison. Because OX_2 was our target at early stages of the current study, the first site-directed mutagenesis campaign focused on the elucidation of the binding mode of the selective hOX_2 EMPA (Malherbe et al., 2009a) and the dual-acting molecule almorexant (Malherbe et al., 2009b) against the human orexin 2 receptor. Carazolol, the partial inverse agonist of human β2-adrenergic receptor, was employed as a template for the locations of EMPA and almorexant. Amino acids, which were found 6.0 Å away from carazolol in the X-ray crystal structure of β2-adrenergic receptor (Cherezov et al., 2007; Rosenbaum et al., 2007), were generally considered possible candidates to affect binding of EMPA and almorexant. Figure 3 shows a set of 17 mutations covering the whole binding site (TM2, -3, -5, -6, -7, and ECL2b) that was suggested from the manual docking of almorexant in the hOX_2 3D homology model. Seventeen residues of OX_2 were mutated to alanine and OX_2 Tyr317$^{6.48}$ was additionally mutated to Phenylalanine to discriminate between its aromatic and hydrogen bond donor capabilities. For OX_1, we selected a smaller list of residues that had been proven to be important for OX_2. Ten residues of OX_1 were mutated to alanine, and OX_1 Ala127$^{3.33}$ was changed to threonine to mimic the OX_2 residue (Fig. 3). Overall, 29 point mutations, 18 in hOX_2 and 11 in hOX_1, were accordingly introduced in the 7TMD region by site-directed mutagenesis.

Effect of Mutations on hOX_1 or hOX_2 Mediation of Orexin-A-Evoked $[Ca^{2+}]_i$ Response. In HEK293 cells transiently expressing hOX_1 or hOX_2, orexin-A (0.0001–10 μM) elicited a concentration-dependent increase in intracellular free calcium $[Ca^{2+}]_i$ as monitored using the Ca^{2+}-sensitive dye Fluo-4 and a FLIPR-96. As seen in Tables 1 and 2, orexin-A activates hOX_2 and hOX_1 with similar potency.

TABLE 1

The effect of mutations on OX_2 mediation of orexin-A-induced $[Ca^{2+}]_i$ response

EC_{50}, Hill slope (n_H), and relative efficacy (E_{max}) values for the orexin-A-induced $[Ca^{2+}]_i$ response in the HEK293 cells transiently transfected with the WT and mutated hOX_2 receptors. The data is mean ± S.E. of eight concentration-response measurements (each performed in duplicate) from four independent transfections. The mutations that affected the potency of orexin-A compared with WT are shown in boldface type.

hOX_2	7TM Position	Orexin-A			
		EC_{50}	EC_{50} (mut)/EC_{50} (WT)	n_H	Relative E_{max}
		nM			
WT		0.6 ± 0.1		0.5 ± 0.0	
T111A	2.61	151.0 ± 22.2	**243.5**	0.7 ± 0.0	114.4 ± 13.0
Q134A	3.32	13.8 ± 2.1	**22.3**	1.4 ± 0.1	62.3 ± 1.1
T135A	3.33	0.5 ± 0.1	0.8	0.6 ± 0.1	109.3 ± 11.2
V138A	3.36	2.8 ± 0.4	4.4	0.7 ± 0.0	92.1 ± 10.0
S139A	3.37	1.5 ± 0.3	2.5	0.6 ± 0.0	86.1 ± 8.6
D211A	45.51	258.0 ± 57.2	**416.1**	0.8 ± 0.1	126.4 ± 16.4
W 214A	45.54	38.7 ± 12.2	**62.4**	0.7 ± 0.1	71.3 ± 7.4
Y223A	5.38	114.0 ± 14.1	**183.9**	1.0 ± 0.1	61.2 ± 1.2
F227A	5.42	149.0 ± 34.8	**240.3**	1.1 ± 0.1	64.3 ± 6.3
F228A	5.43	1.8 ± 0.7	3.0	0.7 ± 0.1	76.2 ± 2.1
Y232A	5.47	17.6 ± 3.1	**28.4**	1.2 ± 0.1	44.9 ± 4.5
Y317A	6.48	11.0 ± 6.1	**17.7**	1.0 ± 0.1	49.6 ± 6.7
Y317F	6.48	0.8 ± 0.3	1.3	0.6 ± 0.1	72.3 ± 9.7
I320A	6.51	0.6 ± 0.2	0.9	0.6 ± 0.0	97.0 ± 5.4
F346A	7.35	33.8 ± 8.8	**54.5**	1.1 ± 0.2	60.7 ± 13.2
H350A	7.39	30.7 ± 5.2	**49.5**	1.1 ± 0.2	63.0 ± 10.7
V353A	7.42	1.2 ± 0.5	1.9	0.6 ± 0.1	84.8 ± 14.7
Y354A	7.43	2.3 ± 0.9	3.7	0.7 ± 0.1	66.1 ± 12.0

TABLE 2

The effect of mutations on OX_1 mediation of orexin-A-induced $[Ca^{2+}]_i$ response

EC_{50}, Hill slope (n_H), and relative efficacy (E_{max}) values for the orexin-A-induced $[Ca^{2+}]_i$ response in the HEK293 cells transiently transfected with the WT and mutated hOX_1 receptors. The data is mean ± S.E. of eight concentration-response measurements (each performed in duplicate) from four independent transfections. The mutations that affected the potency and relative efficacy of orexin-A compared with WT are shown in boldface type.

hOX_1	7TM Position	Orexin-A			
		EC_{50}	EC_{50} (mut)/EC_{50} (WT)	n_H	Relative E_{max}
		nM			
WT		0.9 ± 0.2		0.7 ± 0.1	100
Q126A	3.32	2.2 ± 0.2	2.4	0.7 ± 0.1	59.1 ± 10.1
A127T	3.33	1.6 ± 0.4	1.8	0.8 ± 0.0	97.9 ± 32.9
V130A	3.36	27.5 ± 2.5	**30.6**	0.7 ± 0.1	98.9 ± 31.4
D203A	45.51	367.4 ± 75.0	**408.2**	0.8 ± 0.1	155.2 ± 53.1
W206A	45.54	376.0 ± 102.0	**417.8**	0.8 ± 0.2	45.0 ± 8.0
Y215A	5.38	367.0 ± 95.0	**407.8**	0.6 ± 0.1	65.0 ± 9.0
F219A	5.42	125.6 ± 26.5	**139.6**	0.8 ± 0.1	90.1 ± 48.6
Y224A	5.47	76.0 ± 41.3	**84.4**	0.6 ± 0.1	83.7 ± 40.6
Y311A	6.48	147.5 ± 67.1	**163.9**	0.9 ± 0.1	53.4 ± 12.9
H344A	7.39	217.0 ± 63.9	**241.1**	0.9 ± 0.1	64.5 ± 7.3
Y348A	7.43	7.8 ± 3.0	8.7	0.8 ± 0.0	62.4 ± 18.9

The EC_{50}, n_H, and relative E_{max} values, calculated from concentration-response curves of orexin-A in the cells expressing WT and mutated hOX_2 receptors, are given in Table 1. The mutations $T111A^{2.61}$, $D211A^{45.51}$, $W214A^{5.54}$, $Y223A^{5.38}$, $F227A^{5.42}$, $F346A^{7.35}$, and $H350A^{7.39}$ caused a large decrease in the potency of orexin-A (by 243.5-, 416.1-, 62.4-, 183.9-, 240.3-, 54.5-, and 49.5-fold, respectively) without affecting their efficacy compared with the WT. The mutations $Y232A^{5.47}$ and $Y317A^{6.48}$ resulted in a moderate reduction of both potency (by 28.4-and 17.7-fold, respectively) and efficacy (relative E_{max} of 44.9 and 49.6%, respectively) of orexin-A. The mutation $Q134A^{3.32}$ caused a moderate decrease in potency of orexin-A (by 22.3-fold) without effecting its efficacy.

The effect of mutations on potency (EC_{50}) and efficacy (relative E_{max}) of orexin-A in the HEK293 cells transiently expressing WT and mutated hOX_1 receptors are given in Table 2. The mutations $D203A^{45.51}$, $W206A^{45.54}$, $Y215A^{5.38}$, $F219A^{5.42}$, $Y224A^{5.47}$, $Y311A^{6.48}$, and $H344A^{7.39}$ caused large decreases in the potency of orexin-A (by 408.2-, 417.8-, 407.8-, 139.6-, 84.4-, 163.9- and 241.1-fold, respectively) compared with the WT. Except for the mutation of $W206A^{45.54}$, which caused a moderate decrease in efficacy of orexin-A (relative E_{max} of 45.0%), other mutations had no major effect on efficacy of orexin-A. The mutation $V130A^{3.36}$ moderately affected the potency of orexin-A (30.6-fold) but had no effect on its efficacy.

Effect of Mutations on Binding Affinity and Function Potency of [^{3}H]EMPA and [^{3}H]Almorexant at OX_2 Receptor. To characterize the binding pockets of EMPA and almorexant, 18 point mutations located in the TM2, -3, -5, -6, -7, and ECL2b regions of hOX_2 were selected based on proposed docking mode of almorexant (Fig. 3). With the exception of the $Y232A^{5.47}$ and $Y317A^{6.48}$, which produced a reduction in orexin-A-stimulated fluorescence responses in the FLIPR experiment, the 16 mutations had no effect on or partially affected the orexin-A-induced FLIPR signal. Saturation binding analyses were performed on membranes isolated from the HEK293 transiently transfected with the WT and mutated hOX_2 receptors using 0.01 to 12 nM concentrations of [^{3}H]EMPA or 0.03 to 15 nM concentrations of [^{3}H]almorexant. The dissociation constants (K_d) and the maximum binding sites (B_{max}) derived from the saturation isotherms are given in Table 3.

The mutations $T135A^{3.33}$, $W214A^{45.54}$, $Y223A^{5.38}$, $F227A^{5.42}$, $Y232A^{5.47}$, $Y317A^{6.48}$, $I320A^{6.51}$, $H350A^{7.39}$, and $Y354A^{7.43}$ abolished [^{3}H]EMPA binding to undetectable levels ($K_d > 30$ nM cannot be detected because of high nonspecific binding, NSB > SB). The binding affinity of [^{3}H]EMPA was decreased by 7.4-, 14.9-, 8.7-, and 3.9-fold by mutations $T111A^{2.61}$, $V138A^{3.36}$, $D211A^{45.51}$, and $Y317F^{6.48}$, respectively, and were statistically significant (P = 0.03, 0.0001, 0.003, and 0.002, respectively) (Table 3). In functional FLIPR assay (Fig. 4, A, C, and E, and Table 3), in cells expressing the mutants $T135A^{3.33}$, $W214A^{45.54}$, $Y223A^{5.38}$, $F227A^{5.42}$, $Y232A^{5.47}$, $Y317A^{6.48}$, $I320A^{6.51}$, $H350A^{7.39}$, and $Y354A^{7.43}$, which did not bind [^{3}H]EMPA, EMPA was not able to efficiently inhibit orexin-A-evoked $[Ca^{2+}]_i$ response and thus resulted in the large increases in K_b values (2972.7-, >10,000-, 339.0-, 420.0-, 37.1-, 54.5-, 415.5-, 279.1-, and 366.4-fold, respectively). The mutations $D211A^{45.51}$ and $Y317F^{6.48}$, which caused the decreases in EMPA binding affinity, resulted similarly in decreases of functional potency by 16.8- and 9.5-fold. In general, a good agreement was observed between the effect of mutations on binding affinity and functional potency of EMPA, except for the mutants $T111A^{2.61}$ and $V138A^{3.36}$, in which the effect on functional potency of EMPA was greater than that on binding affinity (51.1- and 90.9-fold increases in K_b values versus 7.4- and 14.9-fold increases in K_d values, respectively).

As seen in Table 3, the mutations $W214A^{45.54}$, $Y223A^{5.38}$, $F227A^{5.42}$, $Y317A^{6.48}$, and $H350A^{7.39}$ abolished [^{3}H]almorexant binding to undetectable levels (K_d, >20 nM cannot be detected because of high nonspecific binding, NSB > SB). The binding affinity of [^{3}H]almorexant was decreased by 10.7- and 10.0-fold by mutations $Q134A^{3.32}$ and $Y232A^{5.47}$, respectively, which were statistically significant (P = 0.04 and 0.006, respectively). It is noteworthy that the mutation $F346A^{7.35}$ caused a 3.25-fold increase in affinity of [^{3}H]almorexant with high statistical significance (P = 0.0002). In functional FLIPR assay (Fig. 4, B, D, and F, and Table 3), in cells expressing the mutants $W214A^{45.54}$, $Y223A^{5.38}$, $F227A^{5.42}$, $Y317A^{6.48}$, and $H350A^{7.39}$ that did not bind [^{3}H]almorexant, almorexant was not able to efficiently inhibit orexin-A-evoked $[Ca^{2+}]_i$ response and thus resulted in the large increases in K_b values (>10,000-, 10,000-, 200.4-, 25.0-, and 94.2-fold, respectively). The mutation $Y232A^{5.47}$, which caused a 10.0-fold decrease in almorexant's binding affinity, resulted similarly in a 7.5-fold decrease of functional potency. Therefore, with the exception of mutation $Q134A^{3.32}$, which led to a decrease in binding affinity (10.7-fold) and had no effect on functional potency, a good correlation between binding and functional potency of almorexant was observed at OX_2.

Comparison of Mutation Effects on Binding and Functional Potencies of SB-674042 and Almorexant at OX_1. To determine the residues forming the binding pockets of SB-674042 and almorexant at hOX_1 receptor, 11 point mutations proposed from docking of almorexant onto OX_1 TM cavity (Fig. 3). Saturation binding analyses were performed on membranes isolated from the HEK293 cells transfected with the WT and mutated OX_1 receptors using 0.03 to 15 nM concentrations of [^{3}H]SB-674042 and 0.02 to 20 nM [^{3}H]almorexant. The dissociation constants (K_d) and the maximum binding sites (B_{max}) derived from the saturation isotherms are given in Table 4. The functional potencies of SB-674042 and almorexant were not measured at $D203A^{45.51}$, $W206A^{45.54}$, and $Y215A^{5.38}$ because of high EC_{80} values (>600 nM) of orexin-A.

As seen in the Table 4, the mutations $W206A^{45.54}$, $Y215A^{5.38}$, and $F219A^{5.42}$ abolished [^{3}H]SB-674042 binding to undetectable levels (K_d > 100 nM cannot be detected because of high nonspecific binding, NSB > SB). The mutants $Q126A^{3.32}$, $A127T^{3.33}$, and $H344A^{7.39}$ caused dramatic decreases in the binding affinity of [^{3}H]SB-674042 by 50.9-, 20.2-, and 22.7-fold, respectively, with high statistical significance (P = 0.0005, 0.003, and 0.0005, respectively). The mutations $Y311A^{6.48}$ and $Y348A^{7.43}$ led to decreases in the binding by 10.8- and 9.3-fold, respectively, and were statistically significant (P = 0.01 and 0.0003, respectively). In the functional FLIPR assay (Fig. 5, A and C, and Table 4), in cells expressing the mutant $F219A^{5.42}$ that did not bind [^{3}H]SB-674042, SB-674042 was not able to efficiently inhibit orexin-A-evoked $[Ca^{2+}]_i$ response and thus resulted in the large increase in K_b value by 311.7-fold. The mutants $Q126A^{3.32}$,

TABLE 3

Comparison of mutation effects on binding and functional potencies of antagonists at OX_2

[^{3}H]EMPA and [^{3}H]almorexant binding properties at human wild-type and mutated hOX_2 receptors. Saturation binding isotherms of [^{3}H]EMPA and [^{3}H]almorexant were performed on membrane preparations from HEK293 cells transiently transfected with the WT and mutated hOX_2 as described under *Materials and Methods*. The K_d and B_{max} values are mean ± S.E., calculated at least from three to five independent experiments (each performed in triplicate). Statistical significance was determined using the two-tailed *t* test. Effects of mutations on inhibition of orexin-A-induced $[Ca^{2+}]_i$ response by EMPA and almorexant. K_b and Hill coefficient (n_H) values for the inhibition by EMPA and almorexant of orexin-A (EC_{80} value)-evoked $[Ca^{2+}]_i$ response in the HEK293 cells transiently transfected with the hOX_2 WT and mutated receptors. Data are means ± S.E. of the six dose-response measurements (each performed in duplicate) from three independent transfections. The mutations that affected the binding and functional potencies of EMPA and almorexant compared with the WT are shown in boldface type.

hOX_2	Position in the 7TMD	[^{3}H]EMPA Binding			EMPA (FLIPR)			[^{3}H]Almorexant Binding			Almorexant (FLIPR)		
		K_d	K_d (mut)/ K_d (WT)	B_{max}	K_b	K_b (mut)/ K_b (WT)	n_H	K_d	K_d (mut)/ K_d (WT)	B_{max}	K_b	K_b (mut)/ K_b (WT)	n_H
		nM		*pmol/mg protein*	*nM*			*nM*		*pmol/mg protein*	*nM*		
WT		1.1 ± 0.0		24.8 ± 0.2	1.1 ± 0.1		0.6 ± 0.0	1.2 ± 0.0		23.1 ± 0.6	2.4 ± 0.1		1.8 ± 0.1
T111A	2.61	8.1 ± 1.9	**7.4***	20.8 ± 3.4	56.2 ± 8.5	**51.1**	0.6 ± 0.1	0.8 ± 0.2	0.7	18.3 ± 2.9	3.4 ± 0.4	1.4	1.1 ± 0.1
Q134A	3.32	1.9 ± 0.3	1.7	4.1 ± 0.2	2.5 ± 0.3	2.3	0.9 ± 0.0	12.8 ± 5.5	**10.7***	18.0 ± 6.1	4.4 ± 0.5	1.8	1.7 ± 0.3
T135A	3.33	**N.D.B.**			3270.0 ± 97.4	**2972.7**	0.6 ± 0.1	1.0 ± 0.2	0.8	11.9 ± 1.3	7.2 ± 0.1	3.0	2.6 ± 0.2
V138A	3.36	16.4 ± 0.8	**14.9*****	18.1 ± 1.4	100.0 ± 12.6	**90.9**	0.6 ± 0.0	1.6 ± 0.1	1.3	18.4 ± 1.8	3.1 ± 0.8	1.3	2.0 ± 0.1
S139A	3.37	1.8 ± 0.1	1.6	4.0 ± 0.3	2.2 ± 0.4	2.0	0.8 ± 0.0	1.8 ± 1.0	1.5	4.5 ± 1.2	3.6 ± 0.6	1.5	2.1 ± 0.1
D211A	45.51	9.6 ± 1.2	**8.7****	11.6 ± 1.0	18.5 ± 2.0	**16.8**	0.7 ± 0.0	0.7 ± 0.2	0.6	9.4 ± 0.9	6.3 ± 0.6	2.6	1.7 ± 0.1
W 214A	45.54	**N.D.B.**			**>10,000**			**N.D.B.**			**>10,000**		
Y223A	5.38	**N.D.B.**			372.9 ± 56.0	**339.0**	3.1 ± 0.9	**N.D.B.**			**>10,000**		
F227A	5.42	**N.D.B.**			462.0 ± 13.9	**420.0**	1.4 ± 0.0	**N.D.B.**			481.0 ± 42.1	**200.4**	0.4 ± 0.1
F228A	5.43	3.3 ± 0.9	3.0	10.1 ± 0.8	3.1 ± 0.6	2.8	0.5 ± 0.1	1.1 ± 0.2	0.9	10.0 ± 1.1	2.6 ± 0.3	1.1	1.6 ± 0.2
Y232A	5.47	**N.D.B.**			40.8 ± 6.5	**37.1**	1.0 ± 0.1	**11.6 ± 1.9**	**10.0****	14.6 ± 2.1	18.1 ± 1.6	**7.5**	1.3 ± 0.2
Y317A	6.48	**N.D.B.**			60.0 ± 7.1	**54.5**	1.0 ± 0.1	**N.D.B.**			59.9 ± 5.1	**25.0**	1.2 ± 0.3
Y317F	6.48	6.2 ± 0.9	**3.9****	12.6 ± 2.5	10.4 ± 0.7	**9.5**	1.0 ± 0.1	1.0 ± 0.0	0.8	5.2 ± 0.1	4.0 ± 0.6	1.7	1.8 ± 0.2
I320A	6.51	**N.D.B.**			457.0 ± 20.9	**415.5**	0.7 ± 0.2	0.8 ± 0.2	0.7	11.2 ± 1.3	3.1 ± 0.8	1.3	1.0 ± 0.2
F346A	7.35	1.6 ± 0.1	1.4	11.8 ± 0.3	1.5 ± 0.2	1.4	1.0 ± 0.0	0.4 ± 0.1	**0.3*****	10.6 ± 0.4	1.9 ± 0.3	0.8	1.5 ± 0.4
H350A	7.39	**N.D.B.**			307.0 ± 35.1	**279.1**	1.0 ± 0.2	**N.D.B.**			**226.0 ± 63.2**	**94.2**	0.5 ± 0.1
V353A	7.42	3.1 ± 0.8	2.8	20.8 ± 2.8	4.4 ± 0.2	4.0	0.7 ± 0.1	3.0 ± 1.1	2.5	20.7 ± 3.6	6.2 ± 0.7	2.6	1.1 ± 0.1
Y354A	7.43	**N.D.B.**			403.0 ± 44.8	**366.4**	0.6 ± 0.1	2.6 ± 0.8	2.2	20.1 ± 2.4	4.7 ± 0.3	2.0	0.9 ± 0.0

N.D.B., no detectable binding due to high nonspecific binding.
* $P < 0.05$.
** $P < 0.01$.
*** $P < 0.001$.

A127T$^{3.33}$, and H344A$^{7.39}$, which caused dramatic decreases in the binding affinity of [^{3}H]SB-674042, similarly led to large decreases in functional potency by 40.3-, 22.8-, and 20.8-fold, respectively. However, the mutations Y311A$^{6.48}$, and Y348A$^{7.43}$, which led to decreases in the binding affinity of SB-674042, had no effect on its functional potency.

As seen in Table 4, the mutations Q126A$^{3.32}$, A127T$^{3.33}$, D203A$^{45.51}$, W206A$^{45.54}$, Y215A$^{5.38}$, F219A$^{5.42}$, Y224A$^{5.47}$, Y311A$^{6.48}$, H344A$^{7.39}$, and Y348A$^{7.43}$ abolished [^{3}H]almorexant binding to undetectable levels (K_d > 20 nM cannot be detected because of high nonspecific binding, NSB > SB). In the functional FLIPR studies (Fig. 5, B and D, and Table 4), in cells expressing the mutants Q126A$^{3.32}$, A127T$^{3.33}$, F219A$^{5.42}$, Y311A$^{6.48}$, H344A$^{7.39}$, and Y348A$^{7.43}$ that did not bind [^{3}H]almorexant, almorexant was not able to efficiently inhibit orexin-A-evoked $[Ca^{2+}]_i$ response and thus resulted in the large increases in K_b values (>10,000-, >10,000-, 191.9-, >10,000-, 61.3-, and 32.7-fold, respectively). However, the mutation Y224A$^{5.47}$, which caused loss of almorexant's binding affinity had a marginal effect on its functional potency.

Docking of SB-674042, Almorexant, and EMPA onto the OX_1-7TMD and OX_2-7TMD Binding Cavities. Our mutational data indicate that the complexes of antagonists with long-lasting pseudo-irreversible mode of antagonism such as almorexant-OX_2 and SB-674042–OX_1 needed fewer contact sites with the respective receptor, whereas the complexes of competitive, reversible antagonists such as EMPA-OX_2 and almorexant-OX_1 were more affected by amino acid replacements, their interactions involving more molecular determinants (Tables 3 and 4). To visualize the mutation data, 3D models of the hOX_1-7TMD and hOX_2-7TMD using the atomic coordinates of hβ2AR (PDB id code 2RH1) were constructed, and three small molecule antagonists were docked onto the transmembrane cavity. Figure 6, A and B, show the docking of almorexant and EMPA to hOX_2. Figure 6C shows both compounds superposed in the hOX_2 binding site. According to the mutational results, both antagonists share important interactions with residues on TM5, -6, and -7. This fits nicely with our predicted docking poses: Tyr223$^{5.38}$, Phe227$^{5.42}$, and Tyr232$^{5.47}$ form a subpocket filled by both antagonists equally well. In addition, both almorexant and EMPA can nicely interact with one of their aromatic rings with His350$^{7.39}$ to form an aromatic π-π interaction. Both antagonists are thus docked onto the same region in the homology model. However, because of their singular chemical structures, they show different effects with further surrounding residues. Most importantly, only the OX_2-selective ligand EMPA was affected by the T135A$^{3.33}$ mutation. This might be explained by the fact that EMPA is located closer to this residue than almorexant and can form a hydrogen bond with the pyridyl group. Besides, only EMPA was affected by the V138A$^{3.36}$, Y317F$^{6.48}$, and Ile320$^{6.51}$ mutations. Fig. 6, B and C, shows that these four residues are located closely to each other deep in the binding cavity and

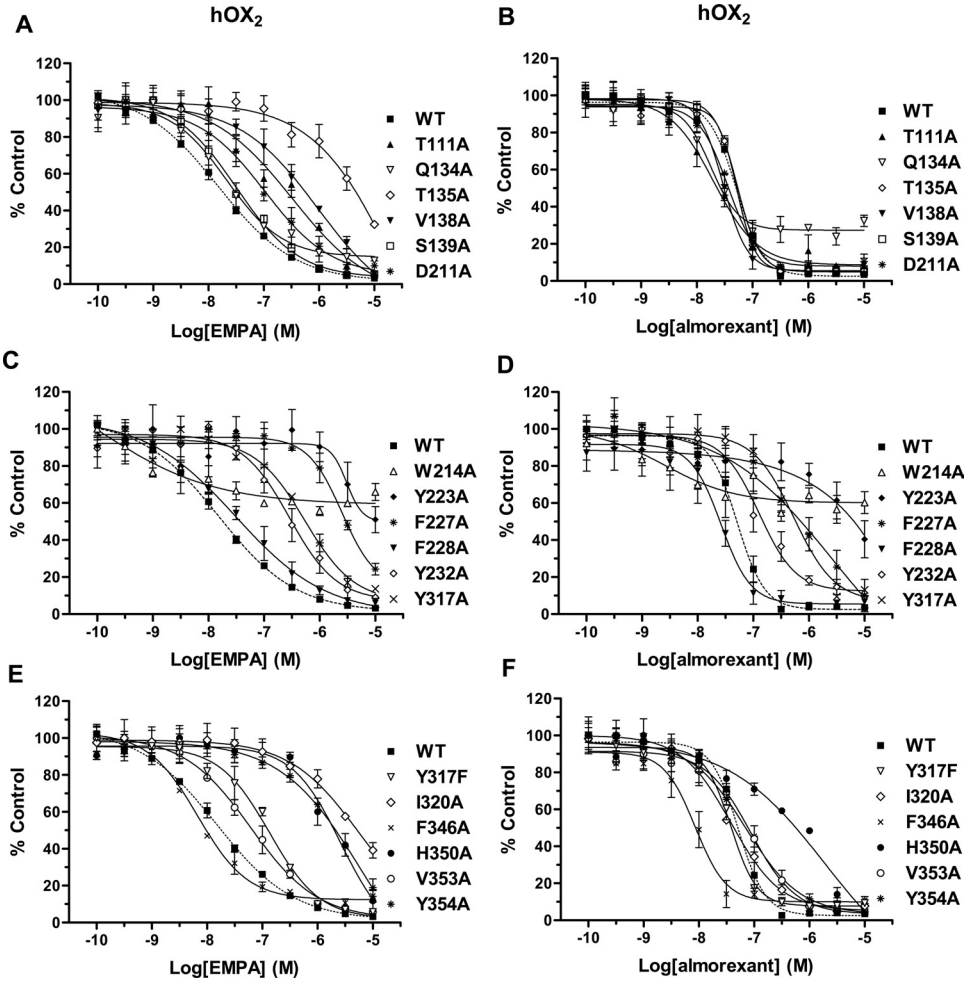

Fig. 4. Effects of orexin antagonists on orexin-A-evoked $[Ca^{2+}]_i$ in WT and mutated hOX_2 receptors. Concentration-dependent inhibition of OX-A (EC_{80} value) stimulated increases in $[Ca^{2+}]_i$ by EMPA (A, C, and E) and almorexant (B, D, and F) as assayed using the Ca^{2+}-sensitive dye Fluo-4 and a fluorometric imaging plate reader in HEK293 cells transiently transfected with the hOX_2 WT and mutated receptors. Responses are normalized to the first control response. Each curve represents the mean of six dose-response measurements (each performed in duplicate) from three independent transfections.

TABLE 4

Comparison of mutation effects on binding and functional potencies of antagonists at OX_1

$[^3H]$SB-674042 and $[^3H]$almorexant binding properties at human wild-type and mutated hOX_1receptors. Saturation binding isotherms of $[^3H]$SB-674042 and $[^3H]$almorexant were performed on membrane preparations from HEK293 cells transiently transfected with the WT and mutated hOX_1 as described under *Materials and Methods*. The K_d and B_{max} values are mean ± S.E., calculated at least from three to five independent experiments (each performed in triplicate). Statistical significance was determined using the two-tailed *t* test. Effects of mutations on inhibition of orexin-A-induced $[Ca^{2+}]_i$ response by SB-674042 and almorexant. K_b and Hill coefficient (n_H) values for the inhibition by SB-674042 and almorexant of orexin-A (EC_{80})-evoked $[Ca^{2+}]_i$ response in the HEK293 cells transiently transfected with the hOX_1 WT and mutated receptors. Data are means ± S.E. of the 6 dose-response measurements (each performed in duplicate) from three independent transfections. The mutations that affected the binding and functional potencies of $[^3H]$SB-674042 and $[^3H]$almorexant compared with the WT are shown in boldface type.

hOX_1	Position in the 7TMD	$[^3H]$SB-674042 Binding			SB-674042 (FLIPR)			$[^3H]$Almorexant Binding			Almorexant (FLIPR)		
		K_d	K_d (mut)/K_d (WT)	B_{max}	K_b	K_b (mut)/K_b (WT)	n_H	K_d	K_d (mut)/K_d (WT)	B_{max}	K_b	K_b (mut)/K_b (WT)	n_H
		nM		*pmol/mg protein*	*nM*			*nM*		*pmol/mg protein*	*nM*		
WT		1.2 ± 0.0		14 ± 0.4	0.6 ± 0.1		0.5 ± 0.1	2.3 ± 0.3		22.9 ± 2.2	4.8 ± 0.7		0.5 ± 0.0
Q126A	3.32	61.1 ± 6.0	**50.9*****	10.0 ± 3.8	24.2 ± 8.8	**40.3**	0.9 ± 0.1	**N.D.B.**			**>10,000**		
A127T	3.33	24.2 ± 7.0	**20.2****	15.2 ± 3.0	13.7 ± 1.6	**22.8**	0.5 ± 0.1	**N.D.B.**			**>10,000**		
V130A	3.36	2.5 ± 1.2	2.1	17.6 ± 0.5	0.6 ± 0.3	1.0	0.7 ± 0.0	3.4 ± 1.0	1.5	13.4 ± 2.3	13.1 ± 1.9	2.7	1.1 ± 0.1
D203A	45.51	0.8 ± 0.1	0.7	9.0 ± 0.2	N.M.			**N.D.B.**			N.M.		
W206A	45.54	**N.D.B.**			N.M.			**N.D.B.**			N.M.		
Y215A	5.38	**N.D.B.**			N.M.			**N.D.B.**			N.M.		
F219A	5.42	**N.D.B.**			187.0 ± 77.1	**311.7**	0.5 ± 0.1	**N.D.B.**			921.0 ± 346.5	**191.9**	0.9 ± 0.3
Y224A	5.47	2.2 ± 1.0	1.8	2.2 ± 0.2	0.3 ± 0.0	0.5	0.6 ± 0.0	**N.D.B.**			22.8 ± 3.7	4.8	0.9 ± 0.1
Y311A	6.48	12.9 ± 3.4	**10.8****	2.7 ± 0.3	0.7 ± 0.1	1.2	0.6 ± 0.0	**N.D.B.**			**>10,000**		
H344A	7.39	27.2 ± 4.0	**22.7*****	1.6 ± 0.8	12.5 ± 1.1	**20.8**	0.8 ± 0.0	**N.D.B.**			294.0 ± 97.1	**61.3**	0.3 ± 0.1
Y348A	7.43	11.2 ± 1.0	**9.3*****	3.2 ± 0.1	4.1 ± 0.6	6.8	0.6 ± 0.1	**N.D.B.**			157.0 ± 18.8	**32.7**	0.8 ± 0.1

N.D.B., no detectable binding due to high nonspecific binding; N.M., not measured.
* $P < 0.05$.
** $P < 0.01$.
*** $P < 0.001$.

are forming a subpocket filled with the *para*-methoxy substituted pyridyl group of EMPA. Almorexant, on the other side, does not reach as deep into this part of the pocket and is thus not influenced by these three mutations. The effect of $F346A^{7.35}$ on only almorexant can be explained by the suboptimal geometry of the edge-to-face aromatic interaction of the phenyl substituent of almorexant with $Phe346^{7.35}$: the aromatic hydrogens of the phenyl substituent of almorexant point onto the aromatic hydrogens of $Phe346^{7.35}$ rather than onto the aromatic face. This is an unfavorable situation. Consequently, removal of the aromatic ring of $Phe346^{7.35}$ results in a statistically significant gain of binding affinity. EMPA is not affected by this mutation because it does not reach close enough to this side chain to form a direct interaction. Furthermore, the effect of $Gln134A^{3.32}$ on almorexant can be explained by a hydrogen bond between $Gln134^{3.32}$ and the amide group in this antagonist. EMPA cannot form such an interaction with these residues. It should be noted that the importance of the $Trp214^{45.54}$ and $Tyr354^{7.43}$ can not be explained from our docking model. $Trp214^{5.54}$ is located on the extracellular loop E2 and is, according to our model, far away from the antagonist binding side. Nevertheless, its location at the entrance of the channel leading to the binding cavity might affect the kinetic characteristics of the antagonists by influencing their entry into the binding site.

Fig. 7A shows the docking of almorexant to hOX_1, which is essentially the same as its docking to the hOX_2 homology model. The only difference between OX_2 and OX_1 in the closer environment of almorexant is $T135A^{3.33}$. It is noteworthy that although the $T135A^{3.33}$ mutation in the OX_2 receptor did not affect almorexant binding, $A127T^{3.33}$ in OX_1 affected almorexant. This cannot be explained from the docking model. However, the introduction of the threonine residue and thus an OH group with its capabilities to form hydrogen bonds might result in a change of the local environment that is different from the OX_2 receptor because of additional differences between OX_2 and OX_1 further away from almorexant. Thus, it might be an indirect effect on almorexant binding and functionality. Finally, Fig. 7B shows a possible docking mode of SB-674042 to hOX_1. It is essentially located in the same region as almorexant. Because it does not come so close to the extracellular loop E2 as almorexant, however, it is not affected by the $D203A^{45.51}$ mutation.

Discussion

Here, we have determined the likely binding pockets of the OX antagonists almorexant, EMPA, and SB-674042 using hβ2AR-based modeling of OX-7TMDs and site-directed mutagenesis. Based on the proposed docking mode of almorexant onto the OX_1- and OX_2-7TMD binding cavities, 29 point mutations (18 in OX_2 and 11 in OX_1) located in the TM2, -3, -5, -6, -7, and ECL2b regions were selected as candidates for mutational studies. The mutated hOX_1 and hOX_2 also made it possible to probe the orexin-A-binding pockets of OX_1 and OX_2 on the basis of orexin-A-evoked $[Ca^{2+}]_i$ response in the HEK293 cells transiently expressing the mutated receptors.

Binding Site of Orexin-A in OX_1 and OX_2. The conserved residues OX_1 $Asp203^{45.51}$ ($Asp211^{45.51}$ in OX_2), $Trp206^{45.54}$ ($Trp214^{45.54}$ in OX_2), $Tyr215^{5.38}$ ($Tyr223^{5.38}$ in OX_2), $Phe219^{5.42}$ ($Phe227^{5.42}$ in OX_2), $Tyr224^{5.47}$ ($Tyr232^{5.47}$ in OX_2), $Tyr311^{6.48}$ ($Tyr317^{6.48}$ in OX_2), and $His344^{7.39}$

(His350$^{7.39}$ in OX_2) were found to be contributing to both orexin-A-binding sites at OX_1 and OX_2, but these residues had yet a more prominent effect on orexin-A potency at OX_1 than that at OX_2. Orexin-A behaved differently on two residues at TM3 helix positions 3.32 and 3.36 between OX_1 and OX_2. The mutation of OX_2 Gln134$^{3.32}$ to alanine caused a 22-fold drop in orexin-A potency at OX_2, whereas the mutation of the corresponding residue in OX_1, Gln126A$^{3.32}$, had no effect on orexin-A potency. Conversely, the mutation OX_1 V130A$^{3.36}$ led to a decrease of 31-fold in orexin-A potency at OX_1 but had no effect on the corresponding residue Val138$^{3.36}$ in OX_2. Therefore, the residues OX_1 Val130$^{3.36}$ and OX_2 Gln134$^{3.32}$ might contribute to the selectivity of orexin-A–OX_1 and –OX_2 binding pockets, respectively. For orexin-A, the conformation and residues required for a high activity at the OX_1 and OX_2 receptors have been extensively characterized. These studies demonstrated that alanine replacement of the same amino acids of orexin-A produced a more prominent reduction in the potency for the OX_1 than that for the OX_2, even though the determinants required

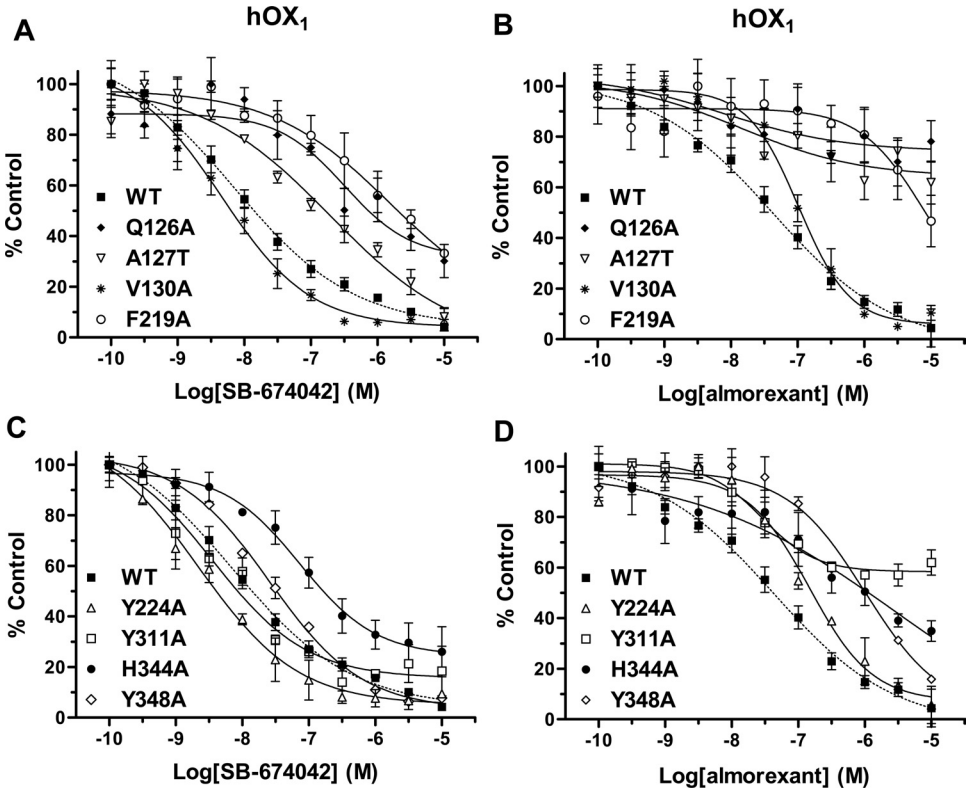

Fig. 5. Effects of orexin antagonists on orexin-A-evoked $[Ca^{2+}]_i$ in WT and mutated hOX_1 receptors. Concentration-dependent inhibition of orexin-A (EC_{80} value) stimulated increases in $[Ca^{2+}]_i$ by SB-674042 (A and C) and almorexant (B and D) as assayed using the Ca^{2+}-sensitive dye, Fluo-4 and a fluorometric imaging plate reader in HEK293 cells transiently transfected with the hOX_1 WT and mutated receptors. Responses are normalized to the first control response. Each curve represents the mean of six dose-response measurements (each performed in duplicate) from three independent transfections.

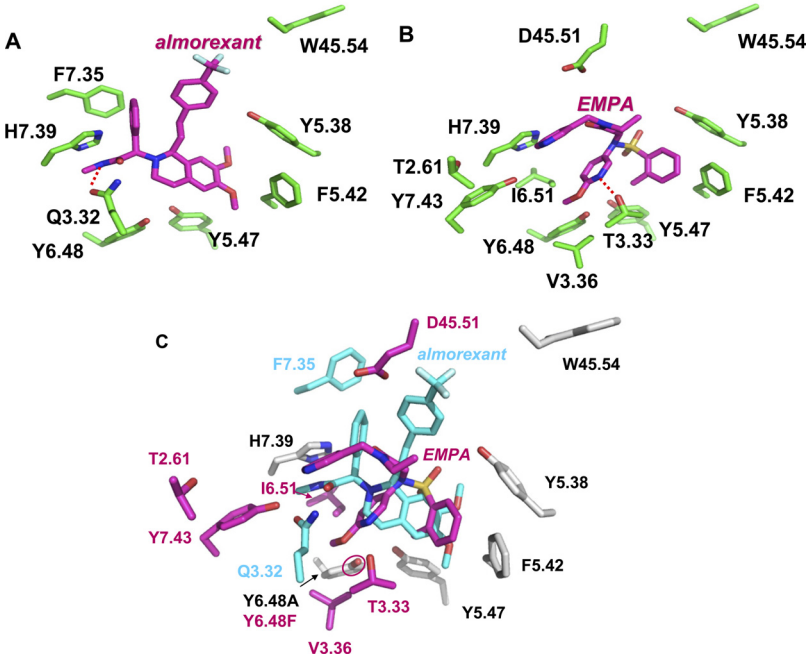

Fig. 6. A and B, predicted docking poses of almorexant (A) and EMPA (B) in the OX_2 binding site. Shown are the residues that were found to be important according to our mutational studies. Ligand carbon atoms are shown in magenta, and protein carbon atoms are shown in green. Blue, nitrogen atoms; red, oxygen; yellow, sulfur; and green, fluorine. The possible hydrogen bond interactions between Gln134$^{3.32}$ with almorexant in A and Thr135$^{3.33}$ with EMPA in B are visualized by red dotted lines. C, predicted docking poses of both almorexant (cyan) and EMPA (magenta) in the OX_2 binding site. Shown in gray are protein carbon atoms of residues that were important for almorexant and EMPA according to our mutational studies. Shown in cyan are protein carbon atoms of residues that were important for only almorexant according to our mutational studies. Shown in magenta are protein carbon atoms of residues that were important for only EMPA according to our mutational studies. Blue, nitrogen atoms; red, oxygen; yellow, sulfur; and green, fluorine.

from orexin-A for activation of the receptor was similar between OX_1 and OX_2 (Ammoun et al., 2003; Lang et al., 2004). The reported observations (that OX_1 was in general more sensitive to amino acid replacements in orexin-A than OX_2) are in good agreement with our mutational studies of OX_1 and OX_2.

Binding Site of OX Antagonists in OX_1 and OX_2. Among 18 point-mutations that are located in TM2, -3, -5, -6, -7, and ECL2b of hOX_2, we observed that the W214A$^{45.54}$, Y223A$^{5.38}$, F227A$^{5.42}$, Y317A$^{6.48}$, and H350A$^{7.39}$ mutations resulted in complete loss of the [^{3}H]EMPA and [^{3}H]almorexant binding affinities and also blocked the inhibition by both antagonists of orexin-A-evoked $[Ca^{2+}]_i$ response. However, the conversion of Tyr317$^{6.48}$ to a phenylalanine had no significant effect on almorexant binding but a small significant effect on EMPA binding affinity. This may indicate that the forces involved in the interaction between Tyr317$^{6.48}$ and almorexant might be via hydrophobic C-H/π interactions. The mutation Y232A$^{5.47}$ led to the complete loss of [^{3}H]EMPA binding affinity and a 37-fold decrease in EMPA potency yet had only a moderate effect on [^{3}H]almorexant binding affinity and potency. It is noteworthy that three mutations, T135A$^{3.33}$, I320A$^{6.51}$, Y354A$^{7.43}$, behaved differently between interacting modes of two antagonists in OX_2, having a detrimental effect on the affinity and potency of EMPA, whereas the affinity and potency of almorexant remained unaffected. Two mutations, T111A$^{2.61}$ and D211A$^{45.51}$, also affected only moderately the binding of EMPA, but not that of almorexant. Of interest is the conserved residue OX_2 Val138$^{3.36}$ (Val130$^{3.36}$ in OX_1): mutation of this residue affected the binding affinity and functional potency of EMPA (15- and 91-fold decreases, respectively), but had no effect on almorexant binding in OX_1 and OX_2 or SB-674042 binding in OX_1. The Val138$^{3.36}$ could be contributing specifically to binding selectivity of EMPA for OX_2. Therefore, it is concluded that the residues Thr135$^{3.33}$ and Val138$^{3.36}$ represent the minimal structural motif responsible for the high selectivity of OX_2 for EMPA. Indeed, in our model, only the EMPA *para*-methoxy substituted pyridyl group can reach deep in the subpocket formed by residues Thr135$^{3.33}$, Val138$^{3.36}$, and Tyr317$^{6.48}$; in addition, its pyridyl ring can form an H-bond with the hydroxyl group of Thr135$^{3.33}$ located in close proximity (Fig. 6B).

Among the 11 point-mutations that are located in TM3, -5, -6, -7, and ECL2b of hOX_1, the mutations Q126A$^{3.32}$, A127T$^{3.33}$, W206A$^{45.54}$, Y215A$^{5.38}$, F219A$^{5.42}$, and H344A$^{7.39}$ abolished the binding affinity and functional potency of both almorexant and SB-674042, yet with a more dramatic effect on almorexant than on SB-674042. The conserved residues Asp203$^{45.51}$, Tyr224$^{5.47}$, Tyr311$^{6.48}$, and Tyr348$^{7.43}$ of OX_1 had completely different behavior between two antagonists: their mutations had detrimental effects on almorexant's binding and function but had little or no effect on SB-674042. The residue at position 3.33 is of special interest, because it

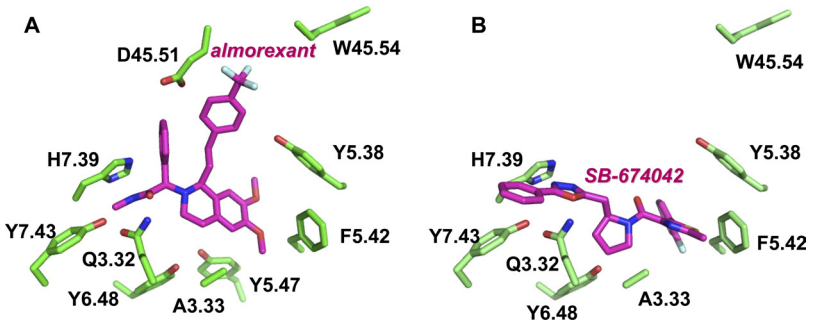

Fig. 7. Predicted docking poses of almorexant (A) and SB674042 (B) in the OX_1 binding site. Shown are the residues that were found to be important according to our mutational studies. Ligand carbon atoms are shown in magenta, and protein carbon atoms are shown in green. Blue, nitrogen atoms; red, oxygen; and green, fluorine.

TABLE 5

Comparison of ligand-binding pocket of orexin receptor antagonists with those of bovine rhodopsin, hβ_2AR, and hA_{2A} adenosine receptor

The residues located at a distance of 4.5 Å from 11-*cis*-retinal (inverse agonist) in the 3D structure of rhodopsin (2.8 Å, PDB id code 1F88) (Palczewski et al., 2000; Teller et al., 2001), within 4 Å of the carazolol (partial inverse agonist) in the 2.4-Å resolution crystal structure of human β2-adrenergic receptor (PDB id code 2RH1) (Cherezov et al., 2007; Rosenbaum et al., 2007), and within 5 Å of the ZM241385 (subtype-selective antagonist) in the 3D structure of human A_{2A} adenosine receptor (2.6 Å, PDB id code 3EML) (Jaakola et al., 2008) are shown for comparison with the critical residues in the binding pocket of orexin receptor antagonists. The generic numbering system proposed by Ballesteros and Weinstein (1995) was used to compare residues in the 7TMD of the different GPCRs.

Position in the 7TMD	Opsd_bovin 11-*cis*-retinal	hβ_2AR Carazolol	hA_{2A} ZM241385	hOX_1		hOX_2	
				SB-674042	Almorexant	Almorexant	EMPA
2.67				N.A.	N.A.	WT	T111A (↓)
3.32	Ala117	Asp113		Q126A (↓)	Q126A (↓)	S. E.	WT
3.33	Thr118	Val114	Leu85	A127T (↓)	A127T (↓)	WT	T135A (↓)
3.36	Gly121	Val117		WT	WT	WT	V138A (↓)
ECL2b (45.51)		Asp192		WT	D203A (↓)	WT	D211A (↓)
ECL2b (45.54)	Tyr191			W206A (↓)	W206A (↓)	W214A (↓)	W214A (↓)
5.38	Phe203	Tyr199	Met177	Y215A (↓)	Y215A (↓)	Y223A (↓)	Y223A (↓)
5.42	Met207	Ser203	Asn181	F219A (↓)	F219A (↓)	F227A (↓)	F227A (↓)
5.47	Phe212	Phe208		WT	Y224A (↓)	Y232A (↓)	Y232A (↓)
6.48	Trp265	Trp286	Trp246	S.E.	Y311A (↓)	Y317A (↓)	Y317A (↓)
6.51	Tyr268	Phe289	Leu249	N.A.	N.A.	WT	I320A (↓)
7.35	Met288	Tyr308	Met270	N.A.	N.A.	F346A (↑)	WT
7.39	Ala292	Asn312	Ile274	H344A (↓)	H344A (↓)	H350A (↓)	H350A (↓)
7.43	Lys296	Tyr316		S.E.	Y348A (↓)	WT	Y354A (↓)

N.A., not available (the mutation was not performed); WT, the same potency as wild type; (↓), decrease in both binding affinity and potency compared with WT; S.E., small but statistically significant decrease in binding affinity; (↑), increase in binding affinity.

is a nonconservative residue between OX_1 (Ala127$^{3.33}$) and OX_2 (Thr135$^{3.33}$). Conversion of Ala127$^{3.33}$ to threonine dramatically affected the binding affinities and functions of SB-674042 and almorexant at OX_1; conversely, conversion of OX_2 Thr135$^{3.33}$ to alanine was detrimental only on EMPA's binding affinity and potency. Hence, the position 3.33 of orexin receptors was identified as a critical position that must be involved in subtype selectivity and also in differentiating two different antagonists for the same receptor, as observed for EMPA and almorexant at OX_2.

Comparison of the Ligand-Binding Site in OX_1 and OX_2 to Other Class A GPCRs. In Table 5, we have summarized our mutational studies of OX antagonists and compared the critical residues contributing to the ligand-binding sites of OX_1 and OX_2 with those of rhodopsin (Palczewski et al., 2000; Teller et al., 2001), hβ_2AR (Cherezov et al., 2007; Rosenbaum et al., 2007), and hA_{2A} (Jaakola et al., 2008). The ligand-binding pockets of OX_1 and OX_2 are very similar and both offer numerous hydrophobic interactions, predominantly aromatic. Besides, the local conformation of positions 3.32, 3.33, and 3.36 in TM3 and 45.51 in ECL2b might provide the structural basis for pharmacologic selectivity between OX_1 and OX_2. It is interesting to note that among seven critical residues that are shared between the orexin-A–OX_1 and –OX_2 binding sites, five residues (Asp$^{45.51}$, Trp$^{45.54}$, Tyr$^{5.38}$, Phe$^{5.42}$, and His$^{7.39}$) are located on the ECL2b and in the top of TM domains at the interface to the main binding crevice, thereby suggesting superficial OX receptor interactions of orexin-A. Similar observation has been reported for other large peptides, such as chemokine receptor interaction with chemokine (Schwarz and Wells, 2002). High-resolution β2AR X-ray structure has revealed that the main ligand-binding pocket is a funnel with a partial lid and that the ECL2b region (highly variable region between the receptors) is an important 7TM structural element forming the edge of this protein lid. In hβ2AR, the formation of a salt bridge between Asp192$^{45.51}$ on ECL2b and Lys305$^{7.32}$ on ECL3 at the extracellular end of TM7 is the major structural feature that blocks access to the ligand binding site. Furthermore, an interaction between Phe193$^{45.53}$ on ECL2b and carazolol was also observed in hβ2AR X-ray structure (Cherezov et al., 2007; Rosenbaum et al., 2007; Ahuja and Smith, 2009). In analogy, OX_1 Asp203$^{45.51}$ (Asp211$^{45.51}$ in OX_2) on ECL2b was found to be crucial for orexin-A–OX_1 and –OX_2, EMPA-OX_2, and almorexant-OX_1 binding sites. The OX_1 Trp206$^{45.54}$ (Trp214$^{45.54}$ in OX_2), another residue located on ECL2b, was also important for OX ligand-binding pocket. Hence, OX receptors might operate with a similar mechanism of activation as β_2AR.

We observed that six OX residues, Trp$^{45.54}$, Tyr$^{5.38}$, Phe$^{5.42}$, Tyr$^{5.47}$, Tyr$^{6.48}$, and His$^{7.39}$, are important contributors to the orexin-A–OX_1 and –OX_2, EMPA–OX_2 and almorexant–OX_1 and –OX_2 binding pockets. We speculate that these aromatic residues are involved in a tight network of interhelical aromatic/hydrophobic interactions, which maintains the OX receptors in a constrained/inactive conformation. Consequently, the OX antagonist, via intramolecular interactions, could further reinforce this network, thereby hindering the structural rearrangements necessary for activation. Of note are the important helix positions 5.47 and 6.48 (Tyr$^{5.47}$ and Tyr$^{6.48}$ in OX), because a recent report investigating ghrelin receptor, β2AR, and NK_1 has demonstrated that two residues, Phe$^{5.47}$ in TM5 and Trp$^{6.48}$ (key residue of the rotamer toggle switch) in TM6, are located in close proximity at the bottom of the main ligand-binding pocket, and an aromatic interaction between two residues could stabilize the active conformation of Trp$^{6.48}$ (Holst et al., 2010). It is noteworthy that two critical residues, Phe$^{5.42}$ and His$^{7.39}$ (in the top of TM5 and TM7), are positioned on opposite extremities of the ligand-binding pocket. In hβ_2AR, the corresponding positions (Ser203$^{5.42}$ and Asn312$^{7.39}$) are involved in H-bond interactions with carazolol (Cherezov et al., 2007; Rosenbaum et al., 2007). Moreover, the position 7.39 in chemokine receptors (Glu$^{7.39}$, a conserved residue among CCRs) provides an important anchor-point for interaction with nonpeptide agonists and antagonists (Rosenkilde and Schwartz, 2006; Jensen et al., 2007). The position 7.39 was also found to be the critical residue in the binding pocket of other peptide receptors, including hNK_2 (Phe293$^{7.39}$), hNK_3 (Phe342$^{7.39}$), hV_{1a} (Ala334$^{7.39}$) and hV_{1b} (Met324$^{7.39}$) (Huang et al., 1995; Derick et al., 2004; Malherbe et al., 2008). In conclusion, we have demonstrated for the first time the important molecular determinants of ligand-binding site of OX_1 and OX_2.

Acknowledgments

We are grateful to Marie-Laure Heusler and Marie-Thérèse Zenner for excellent technical assistance.

References

Ahuja S and Smith SO (2009) Multiple switches in G protein-coupled receptor activation. *Trends Pharmacol Sci* **30:**494–502.
Alexander SP, Mathie A, and Peters JA (2008) Guide to Receptors and Channels (GRAC), 3rd edition. *Br J Pharmacol* **153:**S1–S209.
Ammoun S, Holmqvist T, Shariatmadari R, Oonk HB, Detheux M, Parmentier M, Akerman KE, and Kukkonen JP (2003) Distinct recognition of OX1 and OX2 receptors by orexin peptides. *J Pharmacol Exp Ther* **305:**507–514.
Ballesteros JA and Weinstein H (1995) Integrated methods for construction three-dimensional models and computational probing of structure-function relations in G protein-coupled receptors. *Methods Neurosci* **25:**366–428.
Boss C, Brisbare-Roch C, and Jenck F (2009) Biomedical application of orexin/hypocretin receptor ligands in neuroscience. *J Med Chem* **52:**891–903.
Brisbare-Roch C, Dingemanse J, Koberstein R, Hoever P, Aissaoui H, Flores S, Mueller C, Nayler O, van Gerven J, de Haas SL, et al. (2007) Promotion of sleep by targeting the orexin system in rats, dogs and humans. *Nat Med* **13:**150–155.
Cherezov V, Rosenbaum DM, Hanson MA, Rasmussen SG, Thian FS, Kobilka TS, Choi HJ, Kuhn P, Weis WI, Kobilka BK, et al. (2007) High-resolution crystal structure of an engineered human beta2-adrenergic G protein-coupled receptor. *Science* **318:**1258–1265.
Darker JG, Porter RA, Eggleston DS, Smart D, Brough SJ, Sabido-David C, and Jerman JC (2001) Structure-activity analysis of truncated orexin-A analogues at the orexin-1 receptor. *Bioorg Med Chem Lett* **11:**737–740.
de Lecea L, Kilduff TS, Peyron C, Gao X, Foye PE, Danielson PE, Fukuhara C, Battenberg EL, Gautvik VT, Bartlett FS, et al. (1998) The hypocretins: hypothalamus-specific peptides with neuroexcitatory activity. *Proc Natl Acad Sci USA* **95:**322–327.
Derick S, Pena A, Durroux T, Wagnon J, Serradeil-Le Gal C, Hibert M, Rognan D, and Guillon G (2004) Key amino acids located within the transmembrane domains 5 and 7 account for the pharmacological specificity of the human V1b vasopressin receptor. *Mol Endocrinol* **18:**2777–2789.
Holst B, Nygaard R, Valentin-Hansen L, Bach A, Engelstoft MS, Petersen PS, Frimurer TM, and Schwartz TW (2010) A conserved aromatic lock for the tryptophan rotameric switch in TM-VI of seven-transmembrane receptors. *J Biol Chem* **285:**3973–3985.
Huang RR, Vicario PP, Strader CD, and Fong TM (1995) Identification of residues involved in ligand binding to the neurokinin-2 receptor. *Biochemistry* **34:**10048–10055.
Jaakola VP, Griffith MT, Hanson MA, Cherezov V, Chien EY, Lane JR, Ijzerman AP, and Stevens RC (2008) The 2.6 angstrom crystal structure of a human A2A adenosine receptor bound to an antagonist. *Science* **322:**1211–1217.
Jensen PC, Nygaard R, Thiele S, Elder A, Zhu G, Kolbeck R, Ghosh S, Schwartz TW, and Rosenkilde MM (2007) Molecular interaction of a potent nonpeptide agonist with the chemokine receptor CCR8. *Mol Pharmacol* **72:**327–340.
Kilduff TS and Peyron C (2000) The hypocretin/orexin ligand-receptor system: implications for sleep and sleep disorders. *Trends Neurosci* **23:**359–365.
Lang M, Bufe B, De Pol S, Reiser O, Meyerhof W, and Beck-Sickinger AG (2006) Structural properties of orexins for activation of their receptors. *J Pept Sci* **12:**258–266.
Lang M, Söll RM, Dürrenberger F, Dautzenberg FM, and Beck-Sickinger AG (2004) Structure-activity studies of orexin A and orexin B at the human orexin 1 and

orexin 2 receptors led to orexin 2 receptor selective and orexin 1 receptor preferring ligands. *J Med Chem* **47:**1153–1160.
Langmead CJ, Jerman JC, Brough SJ, Scott C, Porter RA, and Herdon HJ (2004) Characterisation of the binding of [^{3}H]-SB-674042, a novel nonpeptide antagonist, to the human orexin-1 receptor. *Br J Pharmacol* **141:**340–346.
Malherbe P, Bissantz C, Marcuz A, Kratzeisen C, Zenner MT, Wettstein JG, Ratni H, Riemer C, and Spooren W (2008) Me-talnetant and osanetant interact within overlapping but not identical binding pockets in the human tachykinin neurokinin 3 receptor transmembrane domains. *Mol Pharmacol* **73:**1736–1750.
Malherbe P, Borroni E, Gobbi L, Knust H, Nettekoven M, Pinard E, Roche O, Rogers-Evans M, Wettstein JG, and Moreau JL (2009a) Biochemical and behavioural characterization of EMPA, a novel high-affinity, selective antagonist for the OX2 receptor. *Br J Pharmacol* **156:**1326–1341.
Malherbe P, Borroni E, Pinard E, Wettstein JG, and Knoflach F (2009b) Biochemical and electrophysiological characterization of almorexant, a dual orexin 1 receptor (OX1)/orexin 2 receptor (OX2) antagonist: comparison with selective OX1 and OX2 antagonists. *Mol Pharmacol* **76:**618–631.
Marcus JN, Aschkenasi CJ, Lee CE, Chemelli RM, Saper CB, Yanagisawa M, and Elmquist JK (2001) Differential expression of orexin receptors 1 and 2 in the rat brain. *J Comp Neurol* **435:**6–25.
Nambu T, Sakurai T, Mizukami K, Hosoya Y, Yanagisawa M, and Goto K (1999) Distribution of orexin neurons in the adult rat brain. *Brain Res* **827:**243–260.
Neubauer DN (2010) Almorexant, a dual orexin receptor antagonist for the treatment of insomnia. *Curr Opin Investig Drugs* **11:**101–110.
Nishino S (2007) The hypocretin/orexin receptor: therapeutic prospective in sleep disorders. *Expert Opin Investig Drugs* **16:**1785–1797.
Nygaard R, Frimurer TM, Holst B, Rosenkilde MM, and Schwartz TW (2009) Ligand binding and micro-switches in 7TM receptor structures. *Trends Pharmacol Sci* **30:**249–259.
Ohno K and Sakurai T (2008) Orexin neuronal circuitry: role in the regulation of sleep and wakefulness. *Front Neuroendocrinol* **29:**70–87.
Palczewski K, Kumasaka T, Hori T, Behnke CA, Motoshima H, Fox BA, Le Trong I, Teller DC, Okada T, Stenkamp RE, et al. (2000) Crystal structure of rhodopsin: A G protein-coupled receptor. *Science* **289:**739–745.
Peyron C, Tighe DK, van den Pol AN, de Lecea L, Heller HC, Sutcliffe JG, and Kilduff TS (1998) Neurons containing hypocretin (orexin) project to multiple neuronal systems. *J Neurosci* **18:**9996–10015.
Roecker AJ and Coleman PJ (2008) Orexin receptor antagonists: medicinal chemistry and therapeutic potential. *Curr Top Med Chem* **8:**977–987.
Rosenbaum DM, Cherezov V, Hanson MA, Rasmussen SG, Thian FS, Kobilka TS, Choi HJ, Yao XJ, Weis WI, Stevens RC, et al. (2007) GPCR engineering yields high-resolution structural insights into beta2-adrenergic receptor function. *Science* **318:**1266–1273.
Rosenkilde MM and Schwartz TW (2006) GluVII:06—a highly conserved and selective anchor point for non-peptide ligands in chemokine receptors. *Curr Top Med Chem* **6:**1319–1333.
Sakurai T, Amemiya A, Ishii M, Matsuzaki I, Chemelli RM, Tanaka H, Williams SC, Richardson JA, Kozlowski GP, Wilson S, et al. (1998) Orexins and orexin receptors: a family of hypothalamic neuropeptides and G protein-coupled receptors that regulate feeding behavior. *Cell* **92:**573–585.
Schwarz MK and Wells TN (2002) New therapeutics that modulate chemokine networks. *Nat Rev Drug Discov* **1:**347–358.
Takai T, Takaya T, Nakano M, Akutsu H, Nakagawa A, Aimoto S, Nagai K, and Ikegami T (2006) Orexin-A is composed of a highly conserved C-terminal and a specific, hydrophilic N-terminal region, revealing the structural basis of specific recognition by the orexin-1 receptor. *J Pept Sci* **12:**443–454.
Tang J, Chen J, Ramanjaneya M, Punn A, Conner AC, and Randeva HS (2008) The signalling profile of recombinant human orexin-2 receptor. *Cell Signal* **20:**1651–1661.
Teller DC, Okada T, Behnke CA, Palczewski K, and Stenkamp RE (2001) Advances in determination of a high-resolution three-dimensional structure of rhodopsin, a model of G-protein-coupled receptors (GPCRs). *Biochemistry* **40:**7761–7772.
Trivedi P, Yu H, MacNeil DJ, Van der Ploeg LH, and Guan XM (1998) Distribution of orexin receptor mRNA in the rat brain. *FEBS Lett* **438:**71–75.

Address correspondence to: Dr. Pari Malherbe, F. Hoffmann-La Roche Ltd., Bldg. 69/333, CH-4070 Basel, Switzerland. E-mail: parichehr.malherbe@roche.com